





# Dezert-Smarandache Theory-Based Fusion for Human Activity Recognition in Body Sensor Networks

Yilin Dong , Xinde Li , *Senior Member, IEEE*, Jean Dezert, Mohammad Omar Khyam, Md. Noor-A-Rahim , and Shuzhi Sam Ge , *Fellow, IEEE*

**Abstract**—Multisensor fusion strategies have been widely applied in human activity recognition (HAR) in body sensor networks (BSNs). However, the sensory data collected by BSNs systems are often uncertain or even incomplete. Thus, designing a robust and intelligent sensor fusion strategy is necessary for high-quality activity recognition. In this article, Dezert–Smarandache theory (DSmT) is used to develop a novel sensor fusion strategy for HAR in BSNs, which can effectively improve the accuracy of recognition. Specifically, in the training stage, the kernel density estimation (KDE)-based models are first built and then precisely selected for each specific activity according to the proposed discriminative functions. After that, a structure of basic belief assignment (BBA) can be constructed, using the relationship between the test data of unknown class

and the selected KDE models of all considered types of activities. In order to deal with the conflict between the obtained BBAs, proportional conflict redistribution-6 (PCR6) is applied to fuse the acquired BBAs. Moreover, the missing data of the involved sensors are addressed as ignorance in the framework of the DSmT without manual interpolation or intervention. Experimental studies on two real-world activity recognition datasets (The OPPORTUNITY dataset; Daily and Sports Activity Dataset (DSAD)) are conducted, and the results show the superiority of our proposed method over some state-of-the-art approaches proposed in the literature.

**Index Terms**—Belief function theory, DSmT, human activity recognition (HAR), kernel density estimation (KDE), multisensor fusion.

Manuscript received June 14, 2019; revised November 18, 2019 and January 29, 2020; accepted February 17, 2020. Date of publication February 27, 2020; date of current version July 29, 2020. This work was supported in part by the National Natural Science Foundation of China under Grant 61573097 and Grant 91748106, in part by the Key Laboratory of Integrated Automation of Process Industry under Grant PALN201704, in part by the Advanced Research Project of the 13th Five-Year Plan under Grant 31511040301, in part by Science and Technology on Information System Engineering Laboratory, No:05201905, in part by the Fundamental Research Funds for the Central Universities under Grant 3208008401, in part by the Qing Lan Project and Six Major Top-Talent Plan, and in part by the Priority Academic Program Development of Jiangsu Higher Education Institutions. Paper no. TII-19-2507. (Corresponding author: Xinde Li.)

Yilin Dong is with the Key Laboratory of Measurement and Control of CSE, School of Automation, Southeast University, Nanjing 210096, China (e-mail: dyl@seu.edu.cn).

Xinde Li is with the Key Laboratory of Measurement and Control of CSE, School of Automation, Southeast University, Nanjing 210096, China, and also with the School of Cyber Science and Engineering, Southeast University, Nanjing 210096, China (e-mail: xindeli@seu.edu.cn).

Jean Dezert is with the French Aerospace Lab, ONERA, DTIS F-91123, Palaiseau, France (e-mail: jean.dezert@onera.fr).

Mohammad Omar Khyam is with the School of Electrical Engineering, Central Queensland University, Melbourne, VIC 3000, Australia (e-mail: m.khyam@cqu.edu.au).

Md. Noor-A-Rahim is with the School of Computer Science and IT, University College Cork, Cork T12 YN60, Ireland (e-mail: m.rahim@cs.ucc.ie).

Shuzhi Sam Ge is with the Social Robotics Laboratory, Department of Electrical and Computer Engineering, Smart System Institute, National University of Singapore, Singapore 117576, and also with the Institute for Future (IFF), Qingdao University, Qingdao 266071, China (e-mail: samge@nus.edu.sg).

Color versions of one or more of the figures in this article are available online at <http://ieeexplore.ieee.org>.

Digital Object Identifier 10.1109/TII.2020.2976812

## I. INTRODUCTION

**H**UMAN activity recognition (HAR) has spawned intense researches in the past decades and continues to be an active research area [1]–[4]. These HAR systems have enabled several practical applications, such as health monitoring [5], physical activity [6], and gesture detection. Recently, multisensor fusion for activity recognition is playing an increasing role in HAR field and many strategies have been proposed (see [7] for more references). Generally speaking, multisensor fusion strategies can be mainly categorized into three level categories depending on the abstraction level used for data processing: data-fusion level [8], feature-fusion level [9], and decision-level fusion [10]. Among all these three fusion levels, decision-level fusion output is a unique decision obtained from local decision of multiple (homogeneous or heterogeneous) sensors. The fusion in this level has many advantages: communication bandwidth saving, allowing the combination of the heterogeneous sensors. In this article, the main topic thus focus on decision-level fusion area. Two most commonly used approaches for this level of fusion are majority voting [11] and naive Bayes [12]. However, complex sensory data, especially when these data are uncertain or even incomplete, make these two methods unsuitable for HAR. Two classical scenarios are described as follows.

- 1) *Uncertain sensory data in HAR problem*: In order to intuitively discuss the uncertainty of sensory data, one of the involved sensor in university of california irvine (UCI) OPPORTUNITY dataset [13], [14] was randomly selected and parts of the original data of three activities

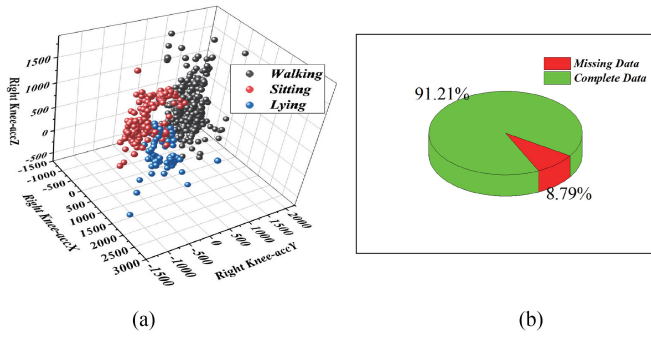


**Fig. 1.** Uncertain and incomplete sensory data in OPPORTUNITY dataset. (a) Uncertain data collected by right knee (RKN) sensor in OPPORTUNITY dataset. (b) Percentage of missing data collected by right knee (RKN) sensor in OPPORTUNITY dataset.

derived from the chosen sensor were drawn in Fig. 1(a). As we can see from Fig. 1(a), some objects that are very close can sometimes truly originate from different classes. Such objects are really difficult to classify correctly into a particular class using the given information. In this case, we call this data uncertain when it can belong to different specific classes with probability mass assignments to estimate.

- 2) *Incomplete sensory data in HAR problem:* Missing data frequently occur during the measurement of wearable-based activity recognition. As we can see in Fig. 1(b), sensory data with incomplete pattern occupy an important proportion which cannot be easily neglected in OPPORTUNITY dataset. The traditional ways to cope with these feature vectors, which include missing data, are to interpolate or delete the whole vector. However, interpolation or deletion is not the wise choice which may bring noise and information loss to the recognition system.

The aforementioned discussions motivate our study, where HAR in body sensor networks (BSNs) is implemented based on belief function theory [15]. Belief function allows to model uncertainty and to fuse basic belief assignments (BBAs) built from sensors' measurements. Within this theory, information fusion relies on the use of a combination rule allowing the pieces of evidences (drawn from sensor readings) expressed in a common frame of discernment to be combined. Among all available combination rules, Dempster's rule proposed by Shafer in Dempster–Shafer theory [15] is the most well-known rule still used in many applications even if it remains very controversial. Recently, Chen *et al.* [16] proposed a new method based on Dempster–Shafer theory to improve human action recognition by using the fusion of depth camera and inertial sensors. Although the recognition results mentioned in [16] is good, two key issues are ignored by authors: 1) In Dempster–Shafer theory, there exists an assumption that hypotheses considered should be exclusive. However, in HAR, activities to be identified often fail to satisfy the characteristics of mutual exclusion. For example, the intersection between “walking” and “running” can be defined as “standing” or intermediate transition state “walking to running” [17]; 2) Dempster's rule cannot solve high conflict issues

and even very low conflict issues in specific cases, which have been widely discussed in [18] and [19].

To solve those mentioned drawbacks in Dempster–Shafer theory, Dezert and Smarandache proposed Dezert–Smarandache theory (DSmT) [18] to solve multisensor fusion problems, with more reasonable assumptions and better combination rules, which is more appropriate to handle HAR problems. In this article, a new use of DSmT is proposed to solve HAR issues thanks to a novel decision-level fusion strategy based on DSmT. Such DSmT-based HAR can be used for online activity recognition system because of its higher recognition accuracy and lower recognition delay, which can meet the required response speed in real-time recognition systems (less than 200 ms) [2]. Specifically, the main contributions of this article are summarized as follows.

- (1) A novel DSmT-based fusion strategy for HAR in BSNs is proposed.
- (2) KDE models are constructed based on the sensor readings, and those selected KDE models of all considered classes are applied to calculate BBAs in DSmT.
- (3) The missing data in original sensor readings are also modeled by vacuous BBA (i.e., the total ignorance source of evidence) in DSmT without any manual interpolation.
- (4) The efficiency of our fusion system with two activities recognition open datasets is demonstrated.

The rest of this article is organized as follows. Section II provides an inventory of the basic concepts of DSmT. Section III provides a description of the new proposed fusion method. Section IV includes the experimental results and discussions. Section V concludes this article.

## II. BASICS OF DSMT

In DSmT framework, the BBAs are defined on the so-called *hyper-power set* (or Dedekind's lattice) denoted  $D^\Theta \triangleq (\Theta, \cup, \cap)$  whose cardinalities follows Dedekind's numbers sequence, see [18], Volume 1 for details and examples. A (generalized) BBA, called a mass function,  $m(\cdot)$  is defined by the mapping:  $D^\Theta \mapsto [0, 1]$ , verifying  $m(\emptyset) = 0$  and  $\sum_{A \in D^\Theta} m(A) = 1$ .

To palliate the drawbacks of Dempster's rule, Martin *et al.* [20] proposed a very interesting combination rule: Proportional conflict redistribution (PCR6). Due to its good performance, it is widely applied in recent applications. We recall that the PCR6 formula for the combination of two BBAs coincides with PCR5 formula originally developed by Smarandache and Dezert in [18]. The combination of two BBAs  $m_1(\cdot)$  and  $m_2(\cdot)$  by the PCR5 rule is given as follows: for  $m_{PCR5}(\emptyset) = 0$  and  $\forall A \in D^\Theta$

$$m_{PCR6}(A) = m_{PCR5}(A) = m_{12}(A) + \sum_{B \in D^\Theta \setminus \{A\} | A \cap B = \emptyset} \left[ \frac{m_1(A)^2 m_2(B)}{m_1(A) + m_2(B)} + \frac{m_2(A)^2 m_1(B)}{m_2(A) + m_1(B)} \right] \quad (1)$$

where  $m_{12}(A) = \sum_{B, C \in D^\Theta | B \cap C = A} m_1(B) m_2(C)$ .

The combinations of more than two BBAs altogether with PCR5 and with PCR6 fusion rule in general provide different results. The choice of PCR6 with respect to PCR5 was justified at first by Martin and Osswald in [20] from a specific application,

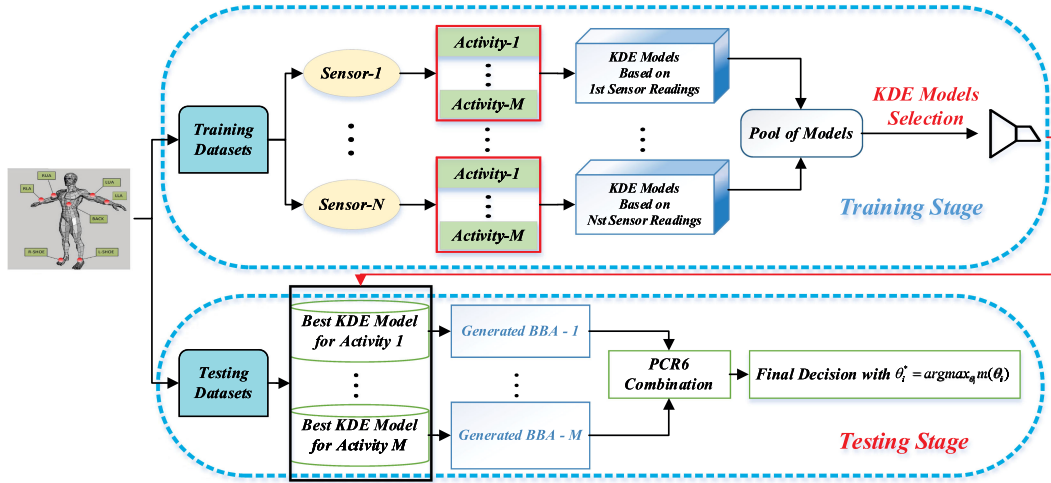


Fig. 2. DSMT-based Fusion strategy for HAR in BSNs.

and then theoretically by Smarandache and Dezert in [21]. The general formula of PCR6 for combining more than two BBAs was given in details in [20] with examples.

### III. DSMT-BASED FUSION STRATEGY FOR HAR IN BSNS

#### A. Flow Chart of Our Proposed Method

Before entering in the detailed presentation of our DSMT-based fusion strategy, we briefly introduce it through the flowchart of Fig. 2 for convenience. Specifically, in the training stage, multiple KDE models are derived from the raw sensor readings so as to build the model pool. Then, the representative model is selected for a particular activity based on our proposed discriminative functions. After that, when the test sample comes, the corresponding BBA is calculated through each activity representative model. Finally, these BBAs are combined with PCR6 rule, from which we make the final decisions.

#### B. Mathematical Definitions of Daily Activities in DSMT

The goal of our work is to recognize human daily activities thanks to DSMT-based framework. Thus, the basic mathematical definitions of the interested activities need to be given. We assume that the finite frame of discernment considered in our activity recognition problem is  $\Theta = \{\theta_1, \theta_2, \dots, \theta_n\}$ . The corresponding hyper-power set of  $\Theta$  is denoted  $D^\Theta$ . Singletons in  $D^\Theta$  are used to represent the simple daily activity such as  $\theta_1 \triangleq$  standing,  $\theta_2 \triangleq$  sitting,  $\theta_3 \triangleq$  lying, and so on. Disjunctive focal elements in  $D^\Theta$  represent the coarse-grained activities. For example,  $\theta_1 \cup \theta_2 \cup \theta_3 \triangleq$  static activity. Also, if  $\theta_4 \triangleq$  walking,  $\theta_5 \triangleq$  running, then  $\theta_4 \cup \theta_5$  is regarded as dynamic activity. Following the definition line of disjunctive focal elements,  $\theta_1 \cup \theta_2 \dots \cup \theta_n$  represents the whole unknown activity. Besides, the conjunctive focal elements in  $D^\Theta$  can be used to stand for the transition activity like  $\theta_1 \cap \theta_2 \triangleq$  standing to sitting or  $\theta_1 \cap \theta_2 \triangleq$  sitting to standing because  $\theta_1 \cap \theta_2 = \theta_2 \cap \theta_1$  and  $\theta_2 \cap \theta_3 \triangleq$  sitting to lying or lying to sitting. In this article, we only consider a restricted hyper-power set, which is denoted as

$D_{\text{restricted}}^\Theta = \{\theta_1, \theta_2, \dots, \theta_n, \theta_1 \cup \theta_2 \dots \cup \theta_n\}$ . In  $D_{\text{restricted}}^\Theta$ , only two types of focal elements exist: one is the singleton, which represents the simple activity and another is  $\theta_1 \cup \theta_2 \dots \cup \theta_n$ , which represents the unknown activity. More complicated situations involving less restricted hyper-power sets will be discussed in our future work.

#### C. Training Model Stage

In the training stage, the KDE model is employed to fit the sensor readings. The most suitable KDE model to distinguish a certain activity is then selected to be regarded as the specific activity representative model. Among the process of this training stage, two main steps are involved as follows.

1) *Construction of KDE Models*: We assume that there are  $M$  kinds of activities that need to be classified and the original dataset collected from the wearable sensors are denoted as  $\mathbf{x}_{ij}$ ,  $i = 1, \dots, M$  and  $j = 1, \dots, N$ . Here,  $M$  represents the types of activities to be classified and  $N$  is the number of sensors. Thus, based on the (2), the KDE model of the specific activity is derived from the sensor readings by

$$f_{ij}(\mathbf{x}_{ij}) = \frac{1}{Q} \cdot \sum_{q=1}^Q K_h(x - x_q^{ij}) = \frac{1}{Qh} \cdot \sum_{q=1}^Q K\left(\frac{x - x_q^{ij}}{h}\right) \quad (2)$$

where  $f(\mathbf{x}_{ij})$  is the KDE model of  $\mathbf{x}_{ij}$  which represents the model of the  $j$  sensor for the  $i$  activity;  $K(\cdot)$  is the kernel function which can be “normal,” “Epanechnikov,” “box,” and “triangle”;  $h$  is the smoothing parameter (the bandwidth) of the KDE model. In this article, the value of  $h$  is the adaptive bandwidth selected by the method presented in [22]; The parameter  $Q$  is the dimension of  $\mathbf{x}_{ij}$ .

2) *Selection of the Best Discriminative KDE Model for the Specific Activity*: As we can see from (2), each activity can have  $N$  KDE models and we need to select the most discriminative KDE model in order to reduce the computational complexity and the interference model. Once the unique KDE model for each activity is selected, one can easily determine a specific sensor



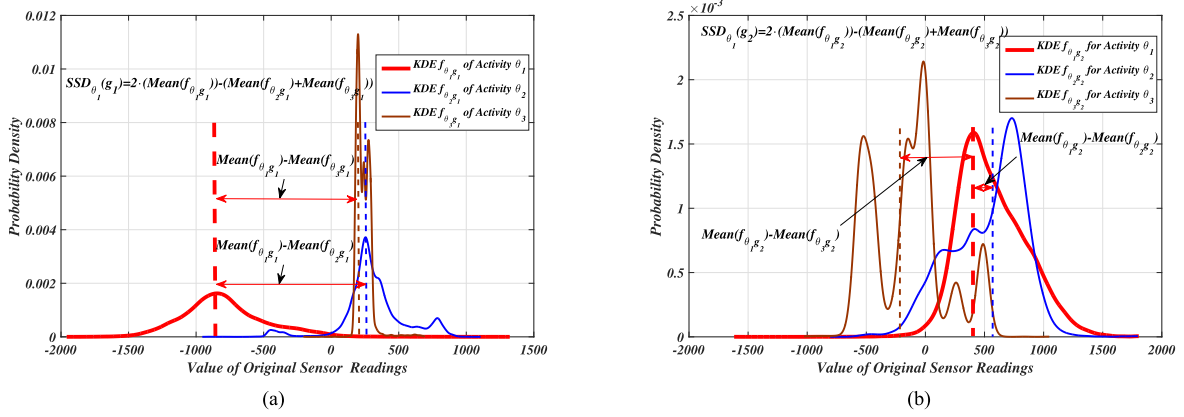


Fig. 3. Selection of the KDE Model for the specific activity based on the principle of SSD function. (a) KDE models of  $g_1$  sensor for three activities  $\theta_1$ ,  $\theta_2$ , and  $\theta_3$ . (b) KDE models of  $g_2$  sensor for three activities  $\theta_1$ ,  $\theta_2$ , and  $\theta_3$ .

to identify activity because there is one-to-one correspondence between the KDE models and the wearable sensors. We propose two novel discriminant evaluation functions as follows.

**Definition 1:** For the specific activity  $\theta_s$ ,  $s \in \{1, \dots, M\}$ , the value of sum of statistical difference (SSD) of the  $j$ ,  $j = 1, \dots, N$  the KDE model is calculated as follows:

$$\begin{aligned} \text{SSD}_{\theta_s}(j) &= [\Psi(f_{\theta_s j}) - \Psi(f_{1j})] + \dots + [\Psi(f_{\theta_s j}) - \Psi(f_{Mj})] \\ &= (M - 1) \cdot \Psi(f_{\theta_s j}) - \sum_{i=1, i \neq s}^M \Psi(f_{\theta_i j}). \end{aligned} \quad (3)$$

In (3),  $\theta_s$  is one of the specific activity among the  $M$  considered activities;  $j$  is the sensor readings of the  $j$  sensor;  $\Psi(\cdot)$  calculates the statistical characteristic value of the derived distribution of the KDE model  $f_{\theta_s j}$ . In this article,  $\Psi(\cdot) = \text{Mean}(\cdot)$ , that is the average value of sensor readings.

The principle of selecting KDE model based on SSD is quite simple: for the specific activity  $\theta_s$ , if the SSD value of the  $j$ ,  $j = 1, \dots, N$  sensor is large, it means that this  $j$  KDE model of  $\theta_s$  has a better discriminative ability. Here, a simple illustrative example was extracted from the OPPORTUNITY dataset experiment in Section IV to show the principle of SSD. As we can see in Fig. 3, for the specific activity  $\theta_1$ , the value of  $\text{SSD}_{\theta_1}(g_1) = (\text{Mean}(f_{\theta_1 g_1}) - \text{Mean}(f_{\theta_2 g_1})) + (\text{Mean}(f_{\theta_1 g_1}) - \text{Mean}(f_{\theta_3 g_1}))$  [Fig. 3(a)] is larger than  $\text{SSD}_{\theta_1}(g_2) = (\text{Mean}(f_{\theta_1 g_2}) - \text{Mean}(f_{\theta_2 g_2})) + (\text{Mean}(f_{\theta_1 g_2}) - \text{Mean}(f_{\theta_3 g_2}))$  [Fig. 3(b)]. Here,  $g_1$  and  $g_2$  represent the  $g_1$  sensor and the  $g_2$  sensor. It can be clearly seen in Fig. 3 that KDE model ( $f_{\theta_1 g_1}$ ) has the higher discriminative ability than KDE model ( $f_{\theta_1 g_2}$ ) for activity  $\theta_1$ .

In order to measure the distances between probability density functions of each pair of KDEs models, another well-known choice for such measurement is Kullback–Leibler (KL) divergence defined by (see [23])

$$\text{Div}_{\text{KL}}(f_{p_1} || f_{p_2}) = \sum_i f_{p_1}(i) \log \frac{f_{p_1}(i)}{f_{p_2}(i)}. \quad (4)$$

Here  $f_{p_1}$  and  $f_{p_2}$  are two discrete probability density functions. Similar to  $\text{Div}_{\text{KL}}$ , another well-known divergence is Jensen–Shannon (JS) divergence defined by

$$\text{Div}_{\text{JS}}(f_{p_1} || f_{p_2}) = \frac{1}{2} [\text{Div}_{\text{KL}}(f_{p_1} || f_{p_2}) + \text{Div}_{\text{KL}}(f_{p_2} || f_{p_1})]. \quad (5)$$

Based on (4) and (5), another discriminative evaluation function is given to measure the discriminative ability between different KDE models, which is named as sum of divergence difference (SDD):

**Definition 2:** For the specific activity  $\theta_s$ ,  $s \in \{1, \dots, M\}$ , the value of SDD of the  $j$ ,  $j = 1, \dots, N$  KDE model is calculated as follows:

$$\text{SDD}_{\theta_s}(j) = \sum_{i, i \neq s}^{M-1} \Upsilon(f_{\theta_s j}, f_{\theta_i j}). \quad (6)$$

In (6),  $\theta_s$  is the specific class of daily activity;  $\Upsilon(\cdot)$  represents the divergence function. In this article,  $\Upsilon(\cdot)$  is defined as KL (4) or JS (5). It is worth noting that in order to make the statements more clear in the following sections, we will directly use the  $\text{Mean}(\cdot)$  to represent that SSD criterion is applied for selecting KDE models in the process of activity recognition. Similarly,  $\text{Div}_{\text{KL}}(\cdot)$  or  $\text{Div}_{\text{JS}}(\cdot)$  mean that SDD is applied and  $\text{Div}_{\text{KL}}(f_{p_1} || f_{p_2})$  or  $\text{Div}_{\text{JS}}(f_{p_1} || f_{p_2})$  is used in SDD criterion to measure the difference between two distributions. For each activity  $\theta_1, \theta_2, \dots, \theta_M$ , the best discriminative  $M$  KDE models  $f_{\theta_i}$ ,  $i = 1, \dots, M$  can be selected and denoted as follows:

$$\begin{bmatrix} f_{\theta_1 g_1} & f_{\theta_2 g_1} & \dots & f_{\theta_M g_1} \\ f_{\theta_1 g_2} & f_{\theta_2 g_2} & \dots & f_{\theta_M g_2} \\ \vdots & \vdots & \ddots & \vdots \\ f_{\theta_1 g_M} & f_{\theta_2 g_M} & \dots & f_{\theta_M g_M} \end{bmatrix} \quad (7)$$

and  $g_1, g_2, \dots, g_M \in [1, N]$ . Each of  $g_i$ ,  $i \in \{1, \dots, M\}$  represents the selected wearable sensor number.

## D. Testing Stage

When the test sample becomes available, the corresponding BBA is calculated through each KDE model of each activity. Finally, we combine all related BBAs with PCR6 rule and we make the final decisions from the combined BBAs.

1) **BBAs Calculation:** In this article, the considered frame of discernment is  $\Theta = \{\theta_1, \theta_2, \dots, \theta_M\}$ . Each focal element in  $\Theta$  represents one kind of activity and here we just consider a simplified  $D_{\text{restricted}}^{\Theta} = \{\theta_1, \theta_2, \dots, \theta_M, \theta_1 \cup \theta_2 \cup \dots \cup \theta_M\}$ . We consider a testing vector  $\mathbf{x}$  with unknown class and we want to identify the label of  $\mathbf{x}$  corresponding to the activity it belongs to. Next, we use the following equations to calculate the BBAs ( $m_1(\cdot), m_2(\cdot), \dots, m_M(\cdot)$ ):

$$m_1(\theta_1) = f_{\theta_1 g_1}(x(g_1)), \dots, m_1(\theta_M) = f_{\theta_M g_1}(x(g_1));$$

$$m_2(\theta_1) = f_{\theta_1 g_2}(x(g_2)), \dots, m_2(\theta_M) = f_{\theta_M g_2}(x(g_2));$$

⋮

$$m_M(\theta_1) = f_{\theta_1 g_M}(x(g_M)), \dots, m_M(\theta_M) = f_{\theta_M g_M}(x(g_M)).$$

It is worth noting that when the value of one feature is missing, we directly assign “1” to  $m(\theta_1 \cup \theta_2 \cup \dots \cup \theta_M)$  which means in this case, we cannot obtain the valuable decision information. Besides, in order to make sure that the derived BBAs satisfy the normalization condition, the following normalization applies:

- (1) If  $m_i(\theta_1) + \dots + m_i(\theta_M) \leq 1$ , then  $m_i(\theta_1 \cup \dots \cup \theta_M) = 1 - (m_i(\theta_1) + \dots + m_i(\theta_M))$ ;
- (2) If  $m_i(\theta_1) + \dots + m_i(\theta_M) > 1$ , then  $m_i(\theta_k) = \frac{m_i(\theta_k)}{\sum_{k=j, \dots, M} m_i(\theta_j)}$  for  $k = 1, \dots, M$ , and  $m_i(\theta_1 \cup \dots \cup \theta_M) = 0$ .

2) **Global Fusion With PCR6 and Decision Making:** After obtaining the  $M$  BBAs, the PCR6 fusion rule is used to fuse all these BBAs which is denoted symbolically by

$$m_{\text{fusion}} = \text{PCR6}(m_1, m_2, \dots, m_M). \quad (8)$$

Then the final decision of the predicted class of  $\mathbf{x}$  can be made as  $\theta_i^* = \text{argmax}_{\theta_i} m_{\text{fusion}}(\theta_i)$ , where  $\theta_i$  is a focal element of the  $D_{\text{restricted}}^{\Theta}$  based on the max of belief mass.

The DSMT-based activity recognition technique is described in Algorithm 1 for convenience.

## IV. PERFORMANCE EVALUATION

### A. Datasets

The performance of the proposed DSMT-Based HAR was evaluated on the following two open HAR datasets. The first one is UCI OPPORTUNITY dataset [13], [14]. The details of this dataset can be found in OPPORTUNITY UCI dataset.<sup>1</sup> Three basic activities were classified: walking, sitting, and lying; The other one is UCI Daily and Sports Activity dataset (DSAD).<sup>2</sup>

<sup>1</sup>[Online]. Available: <http://archive.ics.uci.edu/ml/datasets/OPPORTUNITY+Activity+Recognition>.

<sup>2</sup>[Online]. Available: <http://archive.ics.uci.edu/ml/datasets/Daily+and+Sports+Activities>.

### Algorithm 1: DSMT-Based HAR

---

**Input:** Sequential original data  $\mathbf{x}_{ij}, i = 1, \dots, M, j = 1, \dots, N, K = \text{Normal}'$ .

**Output:** The Predicted Class of Unknown data  $\mathbf{x}^*$ .

- 1 **Initialize:** Cross Validation ( $\mathbf{x}_{ij}$ )  $\rightarrow$   $\mathbf{x}_{\text{training}}, \mathbf{x}_{\text{testing}}$ ;
- 2 **Training Stage:**
- 3 **for**  $i = 1, \dots, M$  **do**
- 4     **for**  $j = 1, \dots, N$  **do**
- 5          $f_{ij}(\mathbf{x}_{ij}) = \frac{1}{Qh} \cdot \sum_{q=1}^Q K(\frac{x-x_{ij}^q}{h})$ ;
- 6     **end**
- 7 **end**
- 8 **for**  $i = 1, \dots, M$  **do**
- 9     **for**  $j = 1, \dots, N$  **do**
- 10          $SSD_{\theta_s}(j) = (M-1) \cdot \Psi(f_{\theta_s j}) - \sum_{i=1, i \neq s}^M \Psi(f_{ij})$ ;
- 11         **or**
- 12          $SDD_{\theta_s}(j) = \sum_{i=1, i \neq s}^{M-1} \Upsilon(f_{\theta_s j}, f_{\theta_i j})$ ;
- 13     **end**
- 14      $g_i = \text{max}(SSD_{\theta_i})$  **or**  $g_i = \text{max}(SDD_{\theta_i})$ ;
- 15 **end**
- 16  $f_{\text{matrix}} =$   
 $f_{\theta_1 g_1}, \dots, f_{\theta_M g_1}; f_{\theta_1 g_2}, \dots, f_{\theta_M g_2}; \dots; f_{\theta_1 g_M}, \dots, f_{\theta_M g_M}$ ;
- 17 **Testing Stage:**
- 18  $D_{\text{restricted}}^{\Theta} = \{\theta_1, \theta_2, \dots, \theta_M, \theta_1 \cup \theta_2 \cup \dots \cup \theta_M\}$ ;
- 19 **for**  $i = 1, \dots, M$  **do**
- 20      $m_i(\theta_1) = f_{\theta_1 g_i}(x^*(g_i)), \dots, m_i(\theta_M) =$   
 $f_{\theta_M g_i}(x^*(g_i))$ ;
- 21 **end**
- 22 **if**  $m_i(\theta_1) + \dots + m_i(\theta_M) \leq 1$  **then**
- 23      $m_i(\theta_1 \cup \theta_2 \cup \dots \cup \theta_M) = 1 - (m_i(\theta_1) + \dots + m_i(\theta_M))$ ;
- 24 **end**
- 25 **else if**  $m_i(\theta_1) + \dots + m_i(\theta_M) > 1$  **then**
- 26     Normalization of BBAs  $m_i(\theta_1), \dots, m_i(\theta_M)$ ;
- 27 **end**
- 28 **Fusion Step:**  $m_{\text{Fusion}} = \text{PCR6}(m_1(\cdot), \dots, m_M(\cdot))$ ;
- 29 **Decision Step:** Take as decision the maximum of belief mass of focal elements  $\theta_i^* = \text{argmax}_{\theta_i} m_{\text{fusion}}(\theta_i)$ ;
- 30 **final** ;
- 31 **return** Predicted Class of  $\mathbf{x}^*$ ;

---

The details of the DSAD can be found in [24]. In this dataset, five common daily activities including sitting, standing, lying, walking, and running were classified to prove the effectiveness of our proposed method.

### B. Measures of Performance

As measures of the performance of our activity recognition system, the classical accuracy, precision, recall, and F1-score [7] have been used. They are defined by

$$\text{Accuracy} = \frac{1}{n} \sum_{k=1}^n \frac{TP_k + TN_k}{TP_k + TN_k + FP_k + FN_k} \quad (9)$$

$$\text{Precision} = \frac{1}{n} \sum_{k=1}^n \frac{TP_k}{TP_k + FP_k} \quad (10)$$

$$\text{Recall} = \frac{1}{n} \sum_{k=1}^n \frac{TP_k}{TP_k + FN_k} \quad (11)$$

$$\text{F1-score} = \frac{1}{n} \sum_{k=1}^n \left( 2 \cdot \frac{\text{precision}_k \cdot \text{recall}_k}{\text{precision}_k + \text{recall}_k} \right) \quad (12)$$

where  $k$  denotes class index and  $n$  is the number of classes. true positives ( $TP_k$ ): the number of correctly recognized class

TABLE I  
SELECTED SENSORS IN OPPORTUNITY DATASET BASED ON  $Mean(\cdot)$ ,  $Div_{KL}(\cdot)$ ,  $Div_{JS}(\cdot)$

Subject	$SSD : \Psi(\cdot) = Mean(\cdot)$			$SDD : \Upsilon_1(\cdot) = Div_{KL}(\cdot)$			$SDD : \Upsilon_2(\cdot) = Div_{JS}(\cdot)$		
	Walking	Sitting	Lying	Walking	Sitting	Lying	Walking	Sitting	Lying
Subject 1	LLA-accX	RLA-accX	Back-magX	LLA-magX	RKN-accZ	Back-magZ	LWR-accY	RKN-accZ	LShoe-accZ
Subject 2	LLA-accX	RLA-accX	LShoe-accZ	LLA-magX	HIP-accY	Back-magZ	RKN-accY	RKN-accZ	Back-magX
Subject 3	RH-accY	LLA-magX	RShoe-accZ	Back-magX	Back-magZ	Back-accZ	RKN-accY	Back-magZ	RShoe-accY
Subject 4	LWR-accY	RH-accY	Back-magX	Back-magZ	LUA-accY	Back-accZ	LUA-accY	LUA-accY	Back-accX

\*According to [25], each triaxial (x, y, z) sensor unit has 3-degree of freedom. And in this table, all the meanings of the involved sensors are: left lower arm (LLA); right lower arm (RLA); right knee (RKN); left wrist (LWR); left Shone (LShone); hips (HIP); right hand (RH); right Shoe (RShoe); left upper arm (LUA); accelerator x-axis (accX); Magnetic z-axis (magZ). More details about OPPORTUNITY dataset can be referred to [25].

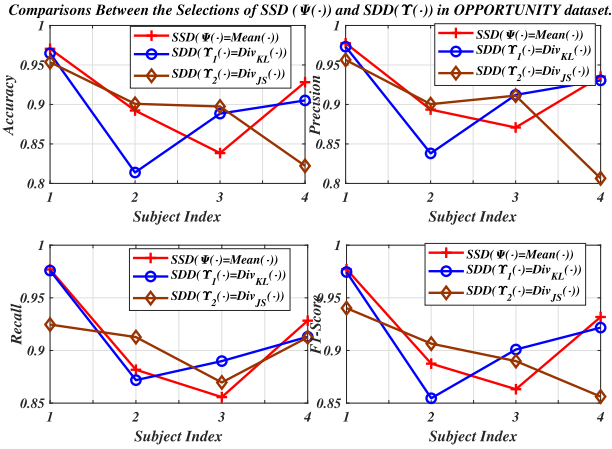


Fig. 4. Effectiveness of the selection of  $SSD(\Psi(\cdot))$  and  $SDD(\Upsilon(\cdot))$  in OPPORTUNITY dataset.

examples; true negatives ( $TN_k$ ): the number of correctly recognized examples that do not belong to the class; false positives ( $FP_k$ ): examples that were either incorrectly assigned to the class; false negatives ( $FN_k$ ): not recognized as class examples.

### C. Results on UCI OPPORTUNITY Dataset

1) *Effectiveness of the Selection of  $\Psi(\cdot)$  and  $\Upsilon(\cdot)$  in (3) and (6)*: The selections of  $\Psi(\cdot)$  in SSD and  $\Upsilon(\cdot)$  in SDD were quite crucial to the representative KDE models for all involved activities. Thus, the relevant comparisons about the recognition rates were given in Fig. 4 when  $\Psi(\cdot)$  and  $\Upsilon(\cdot)$  were set to (1)  $\Psi(\cdot) = Mean(\cdot)$ , (2)  $\Upsilon_1(\cdot) = Div_{KL}(\cdot)$ , (3)  $\Upsilon_2(\cdot) = Div_{JS}(\cdot)$ , respectively. As we can see in Fig. 4, our proposed method based on these three discriminative functions<sup>3</sup> distinguished three mentioned activities in OPPORTUNITY dataset (four subjects) very well, which indirectly proved the effectiveness of  $Mean(\cdot)$ ,  $Div_{KL}$ ,  $Div_{JS}$  in measuring the difference between the distributions of activities. Besides, all the three generated models had the highest recognition accuracy on Subject 1. However, the sensors selected by each function were quite different, and the

corresponding involved sensors were listed in Table I. It can be found that the sensitivity of sensors to different daily activities varied, and was influenced by their locations of deployment. Sensors located on the arm such as left lower arm (LLA), right hand (RH), and left wrist (LWR) were more likely to identify “walking” but sensors located on the Back or shoes had higher recognition rates of “lying” than other sensors. This directly indicates that it is not feasible or wise to rely on a single sensor deployed in a single location to identify various kinds of activities [26]. This is also our motivation to use multisensor fusion strategy based on DS<sub>m</sub>T to solve activity recognition problems.

2) *Recognition Rate Versus Training Percentage*: In this experiment, we did modify the percentage of training set and investigated the relationship between the training percentage and the classification accuracy of our proposed method on OPPORTUNITY dataset. It is worth mentioning that the discriminative function chosen here was SSD (3) and  $\Psi(\cdot) = Mean(\cdot)$ . Since our experiments were conducted based on tenfold cross validation method, it is convenient for us to test the relationship between recognition rate and training percentage. According to the principle of tenfold cross validation, the original datasets were first randomly divided into ten equal parts. And then, in the first experiment, we first treated 10% data as training dataset and the remaining 90% data were used as testing dataset; and in the second experiment, 20% datasets were used for training and the remaining 80% for testing, and so on, until the last experiment which we used 90% datasets for training and the last 10% datasets for testing. Besides, in order to further observe the performance of the proposed method, we divided the original data into 100 equal parts on the basis of 100 cross-validation. And then one of the equal parts was randomly selected as the training datasets (1%) and the remaining (99%) were regarded as testing datasets. The average accuracy rates of all these ten experiments was shown in Fig. 5, which showed that even if there were few training samples, the model proposed in this article still gave higher recognition accuracy.

<sup>3</sup>As we introduced in Definition 1 and Definition 2,  $\Psi(\cdot)$  means that SSD [(3)] is used to choose the best KDE models and  $\Upsilon_1(\cdot)$ ,  $\Upsilon_2(\cdot)$  means that SDD [(6)] is applied in our activity recognition model.

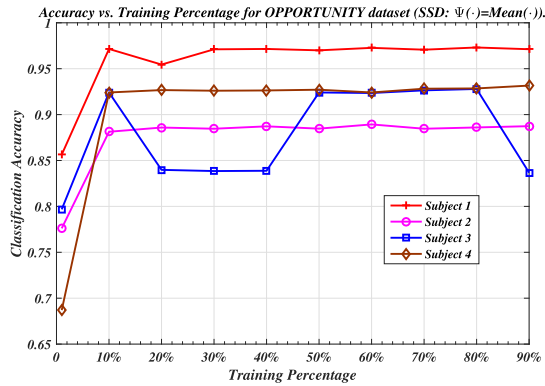


Fig. 5. Classification accuracy versus training percentage for the OPPORTUNITY dataset.

3) *Comparison Between Base Classifiers and Fused Classifiers in OPPORTUNITY Dataset:* In order to deeply analyze the relationship between base classifiers and fused classifier in our proposed model, the detailed comparisons were given in Fig. 6. Based on the results presented in Fig. 4, the discriminative function chosen here was SSD (3) and  $\Psi(\cdot) = \text{Mean}(\cdot)$ . In Fig. 6, the x-axis represents the KDE model corresponding to the selected sensor, the y-axis represents the number of correctly classified test samples, the value above each histogram represents the classification recognition rate corresponding to each KDE model, and the solid line at the top of the histogram represents the total number of test samples. As we can see from Fig. 6: 1) the recognition accuracy of the fused model was significantly improved compared with that of the base classifier; 2) the performance of based classifiers were obviously different. Among these mentioned base classifiers, RH-accY in subject 4 had the lowest rate: 56.9885% and LWR-accY also in subject 4 had the highest rate: 88.7390%. The main reason for the performance difference of the based classifiers is that we looked for the relative *best* KDE model for the specific activity based on our proposed SSD or SDD, not the absolute *best* KDE model for all activities. More concretely, in subject 1, the specific KDE model corresponding to LLA-accX had the best classification only for walking; the specific KDE model corresponding to RLA-accX had the best classification only for sitting and the specific KDE model corresponding to Back-magX had the best classification only for lying. In this way, we could effectively guarantee the degree of diversity among base classifiers, which is really important for ensemble fusion [11].

4) *Comparisons With State-of-the-Art Approaches Based on Monte-Carlo Simulation:* In this part, we further gave the confusion matrix (Fig. 7) of the four subjects in OPPORTUNITY dataset based on our proposed method. It is worth noting that in the confusion matrix of subject 2–4, there existed a special label “UNKNOWN” which was quite different from the three mentioned activities: walking, sitting, and lying. This “UNKNOWN” label occurred in our DSMT-based method because of the missing value in original sensor readings. When the current sensor reading was NULL or missing value, the maximum belief mass (“1”) was assigned to the focal element ( $\Theta$ ) which meant at current time, we really did not know the actual class.

Modeling missing or NULL information is the feature of our proposed method in this article, which is quite different from the traditional supplementation of NULL or missing information by interpolation. In this way, our proposed method can reduce the risk of misjudgment without guaranteeing any changes to the original data. Besides, we repeated 50 experiments and recorded the recognition rates of all four subjects in Table II. Among the mentioned classical approaches, the performance of k-nearest neighbors and nearest centroid classifier were heavily affected by the number of “k”-closest samples and the centroid of each class. These two principles of classification were difficult to work very well when there existed uncertain data in HAR problem. Linear discriminative analysis and quadratic discriminant analysis based on the assumption that the features are normally distributed are obviously unsuitable in HAR problems. Extreme learning machine has been successfully applied for the task of HAR. And for extreme learning machine, sigmoid activation function was utilized and the number of hidden nodes was set to 100. However, due to the randomness of the algorithm, the results of extreme learning machine were unstable and had a wide variability. As we can observe in Table II, our method gave the highest activity recognition accuracy in subject-1, subject-2, and subject-4, and ensemble-extreme learning machine (majority voting) gave the highest recognition accuracy in subject 3. In addition to the comparison of classification accuracy, we also showed the testing time for each individual sample of our proposed method in Table II. Our method was running in MATLAB R2018b with a hardware of Intel Quad Core i5-4670 CPU at 3.4 GHz and 16 G RAM. As shown in Table II, our proposed method was significantly more efficient than other general listed methods. The low recognition delay of our method was mainly because in the testing phase, only the data of selected sensors in the testing sample participates in the BBA calculation. The low-recognition delay also showed its potential for the application in online activity recognition systems, because such real-time activity recognition often requires the predictions are updated 1–5 times/s [2].

#### D. Results on UCI DSAD

1) *Effectiveness of the Selection of  $\Psi(\cdot)$  and  $\Upsilon(\cdot)$  in (3) and (6):* Similar to the discussions in OPPORTUNITY dataset, we also gave the performance comparisons between the selections of  $\Psi(\cdot)$  and  $\Upsilon(\cdot)$  in DSAD. First, the comparisons of recognition accuracy with different evaluation criterion was shown in Fig. 8 when  $\Psi(\cdot)$  and  $\Upsilon(\cdot)$  were set to (1)  $\Psi(\cdot) = \text{Mean}(\cdot)$ , (2)  $\Upsilon_1(\cdot) = \text{Div}_{\text{KL}}(\cdot)$ , (3)  $\Upsilon_2(\cdot) = \text{Div}_{\text{JS}}(\cdot)$ , respectively. Different from the phenomenon in Fig. 4, our proposed method based on  $\text{Div}_{\text{KL}}(\cdot)$  and  $\text{Div}_{\text{JS}}(\cdot)$  could give higher recognition accuracy in DSAD. Due to the robust performance of our proposed method based on  $\Upsilon(\cdot) = \text{Div}_{\text{JS}}(\cdot)$  in DSAD, in the following experiments, the discriminative function  $\text{Div}_{\text{JS}}$  was applied in (6). Besides, the sensors selected by  $\text{Div}_{\text{JS}}$  were also listed in Table III. It can be found that the sensitivity of sensors to different daily activities varied, and was influenced by their locations of deployment and the types of sensors. In Table III, T : Torso; RA : Right Arm; LA : Left Arm; RL : Right Leg; LL : Left Leg; x,



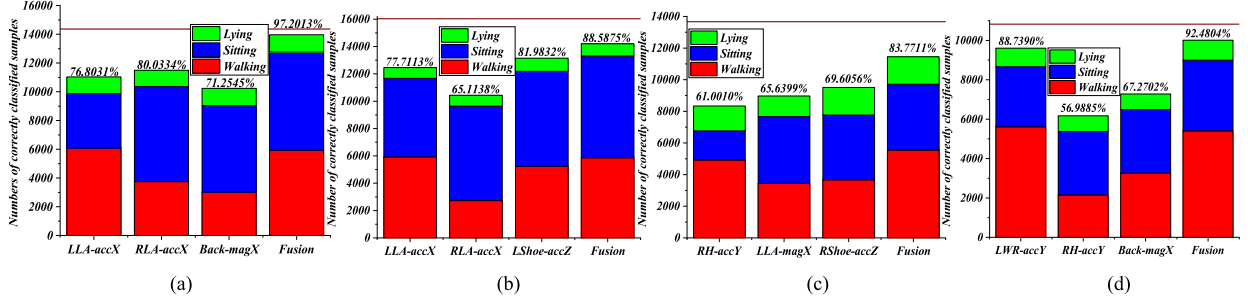


Fig. 6. Comparisons between base classifiers and fused classifiers in OPPORTUNITY dataset. (a) Subject 1. (b) Subject 2. (c) Subject 3. (d) Subject 4.

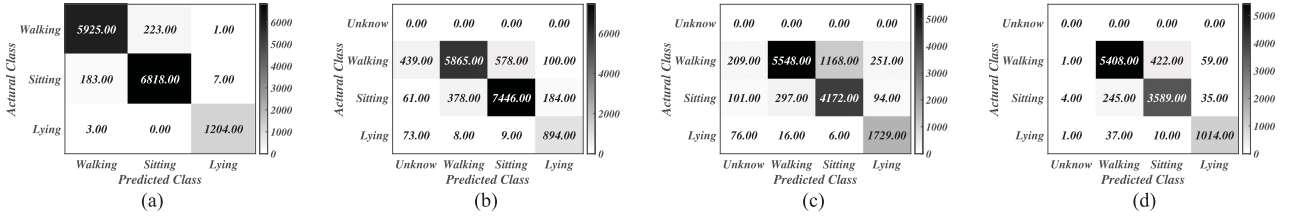


Fig. 7. Confusion matrices of four subjects in OPPORTUNITY dataset. (a) Subject 1. (b) Subject 2. (c) Subject 3. (d) Subject 4.

TABLE II  
COMPARISON WITH STATE-OF-THE-ART RESULTS ON UCI OPPORTUNITY DATASET

Reported Methods	Accuracy				Average Computational Cost
	Subject1	Subject2	Subject3	Subject4	
Extreme Learning Machine [27]	0.7056±0.1123	0.7126±0.0687	0.6587±0.0295	0.7154±0.1414	13.6175 ms
Linear Discriminant Analysis [28]	0.7859±0.0246	0.8147±0.0274	0.7346±0.0318	0.7913±0.0419	11.0537 ms
Nearest Centroid Classifier [14]	0.8305±0.0312	0.8718±0.0289	0.7647±0.0185	0.8185±0.0152	10.3426 ms
K-Nearest Neighbours ( $k = 5$ ) [14]	0.8995±0.0015	0.8516±0.0101	0.8383±0.0291	0.8516±0.0091	11.6340 ms
Quadratic Discriminant Analysis [14]	0.9143±0.0076	0.8517±0.0078	0.8562±0.0218	0.8216±0.0214	13.5754 ms
Naive Bayes [12]	0.8742±0.0015	0.8401±0.0053	0.8210±0.0315	0.8517±0.0091	15.7027 ms
Ensemble-Extreme Learning Machine(Majority Voting) [11]	0.9142±0.0098	0.8843±0.0144	<b>0.8714±0.0156</b>	0.8830±0.0144	29.5384 ms
<b>New Method (HAR DS<sub>m</sub>T-based)</b>	<b>0.9714±0.0014</b>	<b>0.8869±0.0026</b>	0.8439±0.0199	<b>0.9262±0.0025</b>	-
Computational Testing Time For Each Individual Sample	8.6545 ms	14.2733 ms	7.5581 ms	7.6887 ms	9.5436 ms

The bold entities highlight the best experimental results.

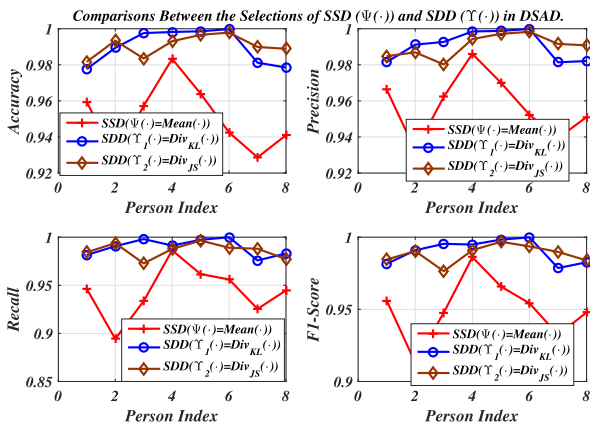


Fig. 8. Effectiveness of the selection of SSD( $\Psi(\cdot)$ ) and SDD( $\Upsilon(\cdot)$ ) in DSAD.

TABLE III  
SELECTED SENSORS IN DSAD BASED ON  $Div_{JS}(\cdot)$

Subject	$SDD : \Upsilon_2(\cdot) = Div_{JS}(\cdot)$				
	Sitting	Standing	Lying	Walking	Running
Person 1	$RA_{zgyro}$	$LA_{zmag}$	$LA_{zacc}$	$LA_{zmag}$	$RA_{xacc}$
Person 2	$RL_{zacc}$	$RA_{ymag}$	$RL_{yacc}$	$LA_{xmag}$	$T_{xgyro}$
Person 3	$T_{yacc}$	$T_{xmag}$	$RA_{yacc}$	$RA_{xmag}$	$LA_{ymag}$
Person 4	$LL_{zacc}$	$RL_{xacc}$	$RA_{yacc}$	$RA_{xmag}$	$LA_{xmag}$
Person 5	$LL_{xmag}$	$LL_{zmag}$	$RL_{yacc}$	$LA_{xmag}$	$LA_{zmag}$
Person 6	$RL_{xmag}$	$RL_{xacc}$	$T_{ygyro}$	$RA_{xacc}$	$T_{zmag}$
Person 7	$RL_{yacc}$	$LL_{xacc}$	$T_{zmag}$	$RA_{zmag}$	$T_{xacc}$
Person 8	$RL_{zacc}$	$LA_{xacc}$	$LA_{zacc}$	$T_{xmag}$	$LA_{ymag}$



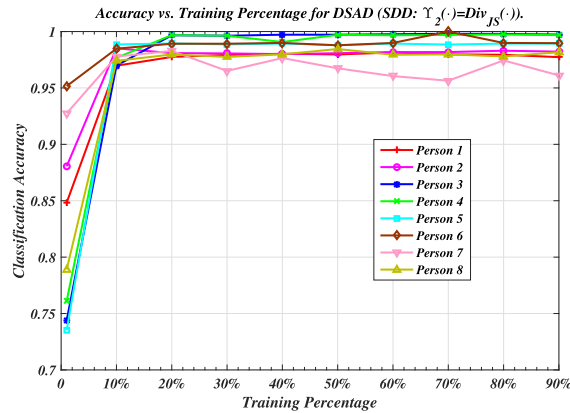


Fig. 9. Classification accuracy versus training percentage for DSAD.

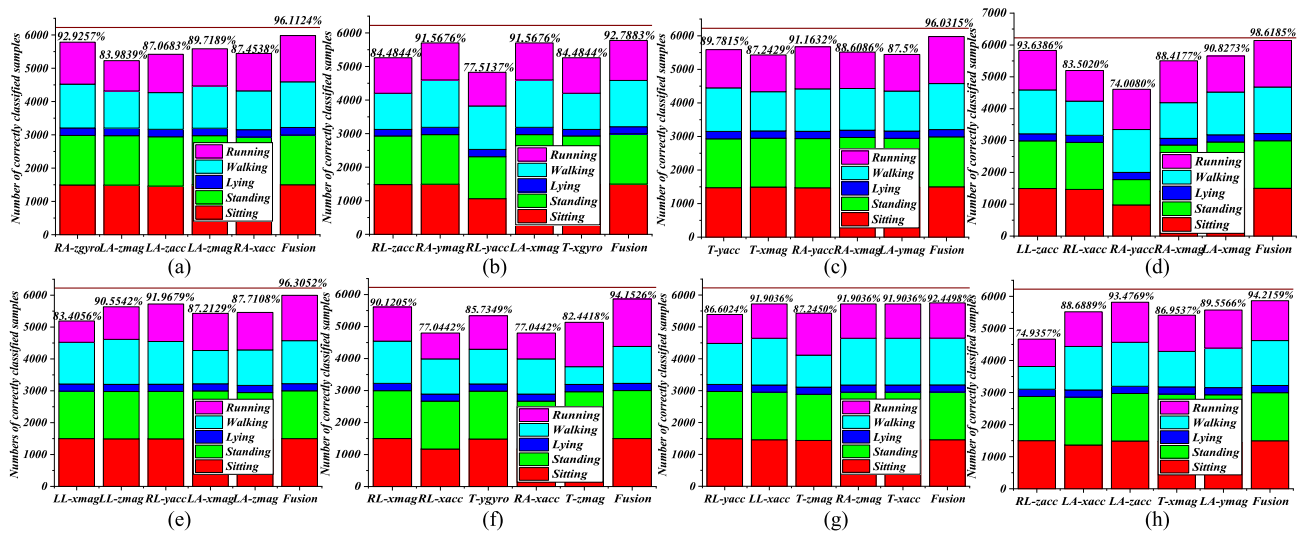


Fig. 10. Comparisons between base classifiers and fused classifiers in DSAD. (a) Person 1. (b) Person 2. (c) Person 3. (d) Person 4. (e) Person 5. (f) Person 6. (g) Person 7. (h) Person 8.

y, zacc: x, y, z accelerometers; x, y, zmag: x, y, z magnetometers; x, y, z gyro: x, y, z gyroscopes.

2) *Recognition Rate Versus Training Percentage*: In this part, we also varied the percentage of training set and investigated the relationship between the training percentage and the classification accuracy of our proposed method on DSAD. Similar to the experiments in OPPORTUNITY dataset, here we also conducted ten independent experiments. The average accuracy rates of all ten experiments can be seen in Fig. 9. From these results, we could also draw the same conclusion as from the proposed method, i.e., classification accuracies for DSAD could reach a high level, without a large amount of training samples.

3) *Comparison Between Base Classifiers and Fused Classifiers in DSAD*: Similar to the experiments in OPPORTUNITY dataset, we also analyzed the relationship between base classifier and fused classifier in DSAD, which was shown in Fig. 10. As we can see from Fig. 10: 1) When the classification difference between base classifiers were quite obvious, the final performance of fused model could be substantially improved.

For example, in person 4, the range of classification accuracy of all base classifiers was [RA-yacc: 74.0080%, LL-zacc: 93.6386%] and the final rate of fused model was 98.6185%; 2) On the contrary, when the performances between base classifiers were close, the performance of final fused model was not substantially improved. For example, in person 7, all five base classifiers had similar recognition rates: 86.6024%, 91.9036%, 87.2459%, 91.9036%, 91.9036%, and the performance of the final fused model was 92.4498%. These two groups of phenomena further verified the rationality of the modeling strategy proposed in this article: base KDE model was only selected for the specific activity, which did guaranty the diversities between base models.

4) *Comparison With State-of-the-Art Approaches Based on Monte-Carlo Simulation*: In this part, we further gave the confusion matrix (Fig. 11) of the eight persons in DSAD based on our proposed method. As we can see in Fig. 11, our method had a higher recognition rate in identifying the activities of all mentioned persons. Besides, we further repeated 50 experiments

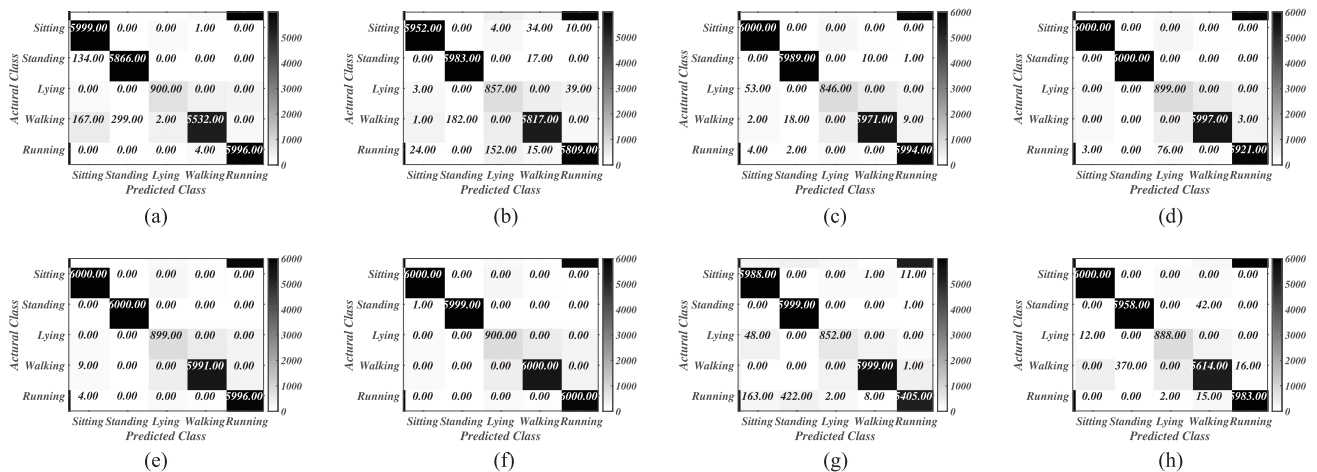


Fig. 11. Confusion matrices of eight persons in DSAD. (a) Person 1. (b) Person 2. (c) Person 3. (d) Person 4. (e) Person 5. (f) Person 6. (g) Person 7. (h) Person 8.

TABLE IV  
COMPARISON WITH STATE-OF-THE-ART RESULTS ON UCI DSAD

Reported Methods	Accuracy	Computational Cost
Artificial Neural Networks [24]	0.743	23.2442 ms
Bayesian Decision Making [24]	0.758	27.4170 ms
K-Nearest Neighbours [24]	0.860	20.2664 ms
Support Vector Machines [24]	0.876	25.9724 ms
differential Recurrent Neural Networks [29]	0.8956	50.9993 ms
pFTA-Learn + K-Nearest Neighbors [30]	0.9018	19.4653 ms
<b>New Method (HAR DSMT-based)</b>	<b>0.9515</b>	17.0964 ms

The bold entities highlight the best experimental results.

and compared DSMT-based method with the other traditional method in references in Table IV. All parameters involved in the mentioned state-of-the-art models were consistent with those mentioned in the literature, which were not listed in detail here. For k-nearest neighbors, the performance of this method changed for different values of  $k$ . A value of  $k = 5$  gave the best results, therefore the accuracy of the k-nearest neighbors algorithm was provided for  $k = 5$  in Table IV. For support vector machine, following the one-versus-the-rest method, each type of activity was assumed as the first class and the remaining four activity types were grouped into the second class. The overall accuracy rate of support vector machine was calculated as 87.6%. Besides, we also conducted performance comparison between our technique and differential recurrent neural networks (dRNN) (the related source codes for dRNN could be downloaded from [29]). As shown in Table IV, our proposed method with DSMT-based fusion strategy could achieve even higher accuracy than traditional approaches. Although support vector machine (SVM) and dRNN were powerful models for classification and they were not able to properly combine the characteristics of multiple sensors; conversely, DSMT-based approach was especially designed to effectively fuse these information from multisensor readings, which proved to be very

effective for HAR in BSNs. Besides, we also showed the testing time for each individual sample of our proposed method in Table IV. Results showed that DSMT-based HAR takes shorter time than other classical methods.

## V. CONCLUSION

In this article, we addressed the challenge of HAR problem in BSNs from the perspective of multisensor fusion strategy and exploited the unique DSMT-Based fusion strategy. In this novel fusion strategy, there were two points worth mentioning: 1) Unlike traditional fusion strategy, not all sensor readings were used for modeling and fusing. Only the selected representative sensors were finally fused; 2) BBA of each test sample was constructed according to KDE models. Besides, the vacuous BBA was directly given when test sample had incomplete pattern. Extensive performance evaluations on two wearable sensor-based HAR datasets (OPPORTUNITY dataset and DSAD) demonstrated that the proposed approach outperformed start-of-the-art methods in accuracy. In our future work, we will explore the performance of the proposed method in complex activity recognition. In this article, our proposed DSMT-based model was trained and tested offline. In our future research works, we will investigate and test how such new model can be applied to an online activity recognition system in real-time.

## ACKNOWLEDGMENT

The authors would like to thank the reviewers and editors for giving valuable comments, which were very helpful for improving this article.

## REFERENCES

- [1] Z. Chen, L. Zhang, and Z. Cao, "Distilling the knowledge from handcrafted features for human activity recognition," *IEEE Trans. Ind. Informat.*, vol. 14, no. 10, pp. 4334–4342, Oct. 2018.
- [2] I. Andrey, "Real-time human activity recognition from accelerometer data using convolutional neural networks," *Appl. Soft Comput.*, vol. 62, pp. 915–922, 2018.

- [3] Z. Chen, Q. Zhu, Y. Soh, and L. Zhang, "Robust human activity recognition using smartphone sensors via CT-PCA and online SVM," *IEEE Trans. Ind. Informat.*, vol. 13, no. 6, pp. 3070–3080, Dec. 2017.
- [4] J. C. Davila, A. M. Cretu, and M. Zaremba, "Wearable sensor data classification for human activity recognition based on an iterative learning framework," *Sensors*, vol. 17, no. 6, pp. 1287–1304, 2017.
- [5] T. G. Lee and S. H. Lee, "Design of wearable bio-patch system platform in human healthcare environment," *Indian J. Sci. Technol.*, vol. 8, no. 17, pp. 751–757, 2015.
- [6] S. A. Khowaja, B. N. Yahya, and S. L. Lee, "Hierarchical classification method based on selective learning of slacked hierarchy for activity recognition systems," *Expert Syst. Appl.*, vol. 88, pp. 165–177, 2017.
- [7] R. Gravina, P. Alinia, H. Ghasemzadeh, and G. Fortino, "Multisensor fusion in body sensor networks: State-of-the-art and research challenges," *Inf. Fusion*, vol. 35, pp. 68–80, 2017.
- [8] D. Schuldhuis, H. Leutheuser, and B. M. Eskofier, "Towards big data for activity recognition: A novel database fusion strategy," in *Proc. 9th Int. Conf. Body Area Netw.*, 2014, pp. 97–103.
- [9] C. Chen, R. Jafari, and N. Kehtarnavaz, "A survey of depth and inertial sensor fusion for human action recognition," *Multimedia Tools Appl.*, vol. 76, no. 3, pp. 1–21, pp. 4405–4425, 2017.
- [10] A. Bulling, U. Blanke, and B. Schiele, "A tutorial on human activity recognition using body-worn inertial sensors," *ACM Comput. Surv.*, vol. 46, no. 3, pp. 1–33, 2014.
- [11] Z. Chen, C. Jiang, and L. Xie, "A novel ensemble ELM for human activity recognition using smartphone sensors," *IEEE Trans. Ind. Informat.*, vol. 15, no. 5, pp. 2691–2699, 2019.
- [12] S. Saeedi and N. El-Sheimy, "Activity recognition using fusion of low-cost sensors on a smartphone for mobile navigation application," *Micromachines*, vol. 6, no. 8, pp. 1100–1134, 2015.
- [13] R. Daniel, C. Alberto, R. Mirco, and H. Thomas, "Collecting complex activity data sets in highly rich networked sensor environments," *Proc. 7th Int. Conf. Networked Sens. Syst.*, 2010, pp. 233–240.
- [14] R. Chavarriaga, H. Sagha, and A. Calatroni, "The opportunity challenge: A benchmark database for on-body sensor-based activity recognition," *Pattern Recognit. Lett.*, vol. 34, pp. 2033–2042, 2013.
- [15] G. Shafer, *A Mathematical Theory of Evidence*, vol. 42. Princeton, NJ, USA: Princeton Univ. Press, 1976.
- [16] C. Chen, R. Jafari, and N. Kehtarnavaz, "Improving human action recognition using fusion of depth camera and inertial sensors," *IEEE Trans. Human-Mach. Syst.*, vol. 45, no. 1, pp. 51–61, Feb. 2015.
- [17] J. L. Reyes-Ortiz, L. Oneto, A. Sam, X. Parra, and D. Anguita, "Transition-aware human activity recognition using smartphones," *Neurocomputing*, vol. 171, pp. 754–767, 2016.
- [18] F. Smarandache and J. Dezert, "Advances and applications of DSMT for information fusion," vol. 1–4, 2004–2015. [Online]. Available: <https://www.onera.fr/staff/jean-dezert/references>
- [19] J. Dezert, P. Wang, and A. Tchamova, "On the validity of Dempster-Shafer theory," in *Proc. Int. Conf. Inf. Fusion*, 2012, pp. 655–660.
- [20] A. Martin and C. Osswald, "A new generalization of the proportional conflict redistribution rule stable in terms of decision," in *Advances and Applications of DSMT for Information Fusion: Collected Works*, Rehoboth: American Research Press, vol. 2, 2006, pp. 69–88.
- [21] F. Smarandache and J. Dezert, "On the consistency of PCR6 with the averaging rule and its application to probability estimation," in *Proc. Int. Conf. Inf. Fusion*, 2013, pp. 1119–1126.
- [22] T. M. Davies, C. R. Flynn, and M. L. Hazelton, "On the utility of asymptotic bandwidth selectors for spatially adaptive kernel density estimation," *Statist. Probability Lett.*, vol. 138, pp. 75–81, 2018.
- [23] K. Stephens and A. G. Bors, "Modelling of interactions for the recognition of activities in groups of people," *Digital Signal Process.*, vol. 79, pp. 34–46, 2018.
- [24] K. Altun, B. Barshan, and O. Tunnl, "Comparative study on classifying human activities with miniature inertial and magnetic sensors," *Pattern Recognit.*, vol. 43, pp. 3605–3620, 2010.
- [25] H. Sagha *et al.*, "Benchmarking classification techniques using the opportunity human activity dataset," in *Proc. IEEE Int. Conf. Syst., Man, Cybern.*, 2011, pp. 233–240.
- [26] A. M. Khan, Y.-K. Lee, S. Y. Lee, and T.-S. Kim, "A triaxial accelerometer-based physical-activity recognition via augmented-signal features and a hierarchical recognizer," *IEEE Trans. Inf. Technol. Biomed.*, vol. 14, no. 5, pp. 1166–1172, Sep. 2010.
- [27] J. Cao, W. Li, C. Ma, and Z. Tao, "Optimizing multisensor deployment via ensemble pruning for wearable activity recognition," *Inf. Fusion*, vol. 41, pp. 68–79, 2018.
- [28] R. Chavarriaga, H. Sagha, and J. D. R. Millan, "Ensemble creation and re-configuration for activity recognition: An information theoretic approach," in *Proc. IEEE Int. Conf. Syst.*, 2011, pp. 2761–2766.
- [29] V. Veeriah, N. Zhuang, and G. J. Qi, "Differential recurrent neural networks for action recognition," in *Proc. IEEE Int. Conf. Comput. Vis.*, 2015, pp. 4041–4049.
- [30] J. Ye, G. Qi, N. Zhuang, H. Hu, and K. A. Hua, "Learning compact features for human activity recognition via probabilistic first-take-all," *IEEE Trans. Pattern Anal. Mach. Intell.*, vol. 42, no. 1, pp. 126–139, Jan. 2020.



**Yilin Dong** was born in Yancheng, China, in 1990. He received the Ph.D. degree in control science and engineering from the School of Automation, Southeast University, Nanjing, China, in 2020.

His research interests include belief function theory, information fusion, and pattern recognition.



**Xinde Li** (Senior Member, IEEE) received the Ph.D. degree in control theory and control engineering, from the Department of Control Science and Engineering, Huazhong University of Science and Technology (HUST), Wuhan, China, in 2007.

After receiving Ph.D. degree, he joined School of Automation, Southeast University, Nanjing, China. During the period from 2012 to 2013, he was a Visiting Scholar with School of Interactive Computing, Georgia Institute of

Technology, Atlanta, GA, USA. In 2016, he was a Postdoc Research Fellow with Department of Electrical and Computer Engineering, National University of Singapore, Singapore. He is currently a Professor and Ph.D. Supervisor with Department of Control Science and Engineering, Huazhong University of Science and Technology (HUST). His research interests include information fusion, object recognition, computer vision, intelligent robot, and human-robot interaction.

Dr. Li was granted a Talent of Qing Lan Project Award of Jiangsu province and a Six Major Top-talent Plan Award of Jiangsu province, China.



**Jean Dezert** was born in LHay les Roses, France, in 1962. He received the degree in electrical engineering from the Ecole Française de Radioélectrique Electronique et Informatique, Paris, France, in 1985, and the Ph.D. degree in automatic control and signal processing from the University Paris XI, Orsay, France, in 1990.

Since 1993, he has been a Senior Research Scientist with the Information Modeling and Processing Department, ONERA, Palaiseau, France. His current research interests include

belief function theory, particularly for DSMT, which he has developed with Prof. Smarandache.



**Mohammad Omar Khyam** received the B.Sc. degree in electronics and telecommunication engineering from the Rajshahi University of Engineering and Technology, Rajshahi, Bangladesh, in 2010, and the Ph.D. degree in electrical engineering from the University of New South Wales, Sydney, NSW, Australia, in 2015.

He is currently a Lecturer with Electrical Engineering, School of Engineering and Technology, the Central Queensland University, Melbourne,

VIC, Australia. His research interests include signal processing and wireless communication.



**Md. Noor-A-Rahim** received the Ph.D. degree in telecommunications from the Institute for Telecommunications Research, University of South Australia, Adelaide, SA, Australia, in 2015.

He was a Postdoctoral Research Fellow with the Centre for Infocomm Technology, Nanyang Technological University, Singapore. He is currently a Senior Postdoctoral Researcher (MSCA Fellow) with the School of Computer Science and IT, University College Cork, Cork, Ireland.

His research interests include control over wireless networks, intelligent transportation systems, information theory, signal processing, and DNA-based data storage.

Dr. Noor-A-Rahim was the recipient of the Michael Miller Medal from the Institute for Telecommunications Research, University of South Australia, for the most Outstanding Ph.D. thesis, in 2015.



**Shuzhi Sam Ge** (Fellow, IEEE) received the B.Sc. and M.Sc. degrees in control engineering from Beijing University of Aeronautics and Astronautics, Beijing, China, in 1986 and 1988, respectively, and the Ph.D. degree in mechanical/electrical engineering from the Imperial College of Science, Technology and Medicine, University of London, London, U.K., in 1993.

He is currently the Founding Director of the Robotics Institute and the Institute of Intelligent Systems and Information Technology, University of Electronic Science and Technology of China, Chengdu, China. He is also the Founding Director of the Social Robotics Laboratory, Interactive Digital Media Institute, National University of Singapore, Singapore, where he is a Professor with the Department of Electrical and Computer Engineering.

Dr. Ge is the Editor-in-Chief of the *International Journal of Social Robotics*. He has served as an Associate Editor for a number of flagship journals. He has also served as the Vice-President of Technical Activities, from 2009 to 2010; Membership Activities, from 2011 to 2012; and the IEEE Control Systems Society.